Neuron
Report

# Traveling Theta Waves along the Entire Septotemporal Axis of the Hippocampus

Jagdish Patel,[1] Shigeyoshi Fujisawa,[1] Antal Berényi,[1,2] Sébastien Royer,[1,3] and György Buzsáki[1,4,*]
[1]Center for Molecular and Behavioral Neuroscience, Rutgers, The State University of New Jersey, 197 University Avenue, Newark, NJ 07102, USA
[2]University of Szeged, Department of Physiology, 10 Dom Square, Szeged, H-6720, Hungary
[3]Center for Functional Connectomics, Korea Institute of Science and Technology, Seoul-136-791, Republic of Korea
[4]NYU Neuroscience Institute, New York University School of Medicine, East Rivers Science Park, 450 East 29th Street, 9th Floor, New York, NY 10016, USA
*Correspondence: gyorgy.buzsaki@nyumc.org
http://dx.doi.org/10.1016/j.neuron.2012.07.015

## SUMMARY

**A topographical relationship exists between the hippocampus-entorhinal cortex and the neocortex. However, it is not known how these anatomical connections are utilized during information exchange and behavior. We recorded theta oscillations along the entire extent of the septotemporal axis of the hippocampal CA1 pyramidal layer. While the frequency of theta oscillation remained same along the entire long axis, the amplitude and coherence between recording sites decreased from dorsal to ventral hippocampus (VH). Theta phase shifted monotonically with distance along the longitudinal axis, reaching ~180° between the septal and temporal poles. The majority of concurrently recorded units were phase-locked to the local field theta at all dorsoventral segments. The power of VH theta had only a weak correlation with locomotion velocity, and its amplitude varied largely independently from theta in the dorsal part. Thus, theta oscillations can temporally combine or segregate neocortical representations along the septotemporal axis of the hippocampus.**

## INTRODUCTION

The elongated hippocampus communicates with the neocortex via the entorhinal cortex interface (Witter et al., 1989). Both hippocampal "representation" of neocortical information and rerouting of hippocampal messages to the neocortex are topographically organized (cf. Amaral and Lavenex, 2007; Witter et al., 1989). The septal (or "dorsal," DH) and intermediate (IH, or posterior) segments receive visuospatial inputs indirectly mainly via the dorsolateral band of the medial entorhinal cortex, while the temporal segment (or "ventral hippocampus," VH) from the ventromedial band of the entorhinal cortex (Dolorfo and Amaral, 1998; Witter et al., 1989). In addition, the temporal segment is innervated by amygdalar and hypothalamic afferents carrying emotional and other nonspatial information (Risold and Swanson, 1996; Petrovich et al., 2001) and has characteristically distinct gene profiles (Thompson et al., 2008; Dong et al., 2009). In return, the septal and temporal segments of the hippocampus broadcast to different streams of structures (Amaral and Lavenex, 2007; Cenquizca and Swanson, 2007). In contrast to its afferent and efferent connections, the internal organization of the hippocampus suggests that the widespread neocortical representations are integrated (cf., Bannerman et al., 2003; Bast et al., 2009; Kjelstrup et al., 2002; Moser et al., 2008; Small, 2002; Royer et al., 2010) by the extensive recurrent collateral system of CA3 pyramidal neurons (Ishizuka et al., 1990; Li et al., 1994).

The physiological mechanisms of communication between the hippocampus and the neocortex are not well understood. Neuronal recording studies from the septal and more temporal segments of the hippocampus are controversial and range from emphasizing the unity of hippocampal operations (O'Keefe and Nadel, 1978; Bullock et al., 1990; Jung et al., 1994; Kjelstrup et al., 2008; Lubenov and Siapas, 2009; Maurer et al., 2005) to more localized and specialized computations (Hampson et al., 1999; Royer et al., 2010; Segal et al., 2010; Wiener, 1996). A fundamental mode of hippocampal operations is reflected by theta oscillations during explorative behavior and REM sleep (4–10 Hz; cf., Buzsáki, 2002). In a recent elegant study Lubenov and Siapas (2009) have observed that the phase of theta waves advances systematically in the dorsal hippocampus (Lubenov and Siapas, 2009) and hypothesized a full cycle (i.e., 360°) phase shift between the septal and temporal poles. The implication of a full-cycle phase shift of theta waves is that outputs from the two poles of the hippocampus would affect their joint targets in a temporally synchronous manner, while the intermediate parts would remain temporally segregated from either pole. To examine the spatial organization of theta patterns, we recorded LFP and neuronal discharge activity in the subiculofimbrial (transverse) axis and from the entire length of the septotemporal (longitudinal) axis of the hippocampal CA1 pyramidal layer during behavioral exploration and REM sleep.

## RESULTS

LFP and unit activity were recorded during REM sleep in the home cage and during navigation (RUN sessions) either while

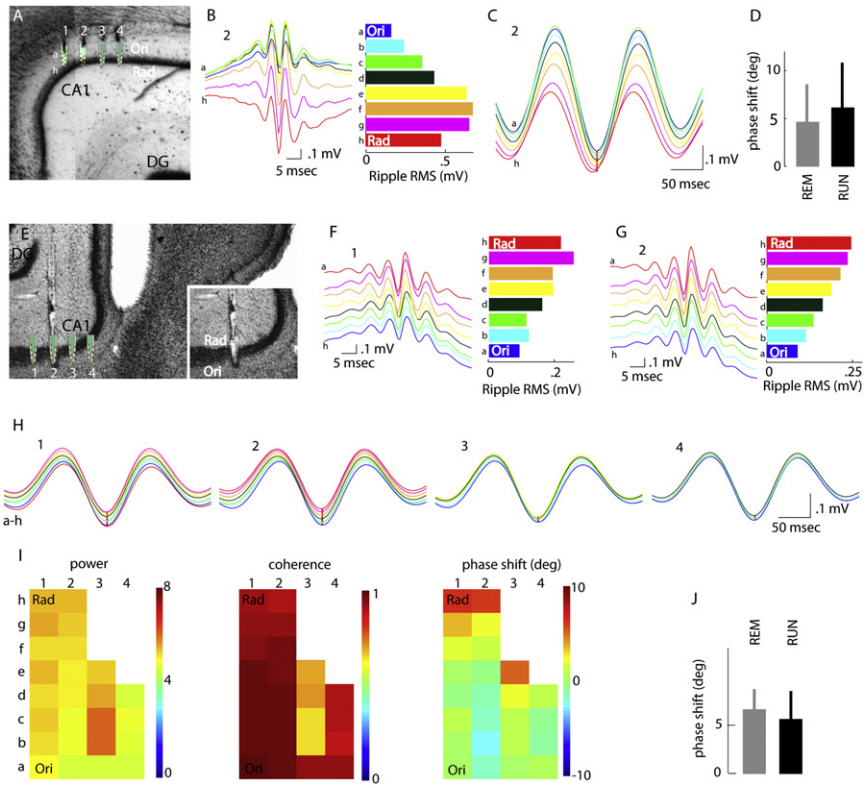


**Figure 1. Similar Theta Phases in the Stratum Oriens and Pyramidale of Both Dorsal and Ventral Hippocampus**

(A) Four-shank silicon probe tips superimposed on the histologically recovered tracks. Ori, stratum oriens. Rad, stratum radiatum. (B) Average filtered (100–250 Hz) ripple traces from each of the eight recording sites (on shank 2) triggered by ripple troughs. Right, ripple power at each recording site. The recording site with the largest ripple power identifies the middle of the pyramidal layer. (C) Averaged filtered (5–10 Hz) theta waves during REM, from the same sites in the same session. Same color-coding as in (B). (D) Mean (+ SD) theta phase shift between midpyramidal layer and str. oriens locations (REM: n = 41 pairs from eight sessions in six rats; RUN: n = 62 pairs from ten sessions in five rats). (E) Four-shank silicon probe in the CA1 pyramidal layer of ventral hippocampus. (F and G) Average filtered ripples and ripple power at all sites of shank 1 (F) and 2 (G). (H) Average filtered theta waves recorded from all good channels on each of the four shanks. Averages recorded by the same shank are superimposed. (I) Power, coherence, and phase difference as a function of depth (eight sites; 20 μm intervals) and lateral distance (shanks are 200 μm apart). Malfunctioning sites are white. (J) Mean (+ SD) theta phase shift between midpyramidal layer and str. oriens locations (REM: n = 40 pairs from 14 sessions in three rats; RUN: n = 22 pairs from eight sessions in three rats).

the rat was chasing small fragments of randomly dispersed froot loops on an open field and/or running for a water reward in an 11-compartment zig-zag maze (Royer et al., 2010). Since the phase of theta oscillation in the CA1 region varies along the somatodendritic (depth), subicular-CA3 (transverse), and septotemporal (dorsoventral or longitudinal) axes (Buzsáki, 2002; Lubenov and Siapas, 2009; Patel et al., 2008, Soc. Neurosci., abstract, 435.13), we examined phase shifts in each direction using multiple site silicon probes and independently movable wire electrode arrays (see Experimental Procedures). Theta phase difference between the alveus and the CA1 pyramidal layer in both the dorsal (Figures 1A–1D) and ventral (Figures 1E–1J) segments of the hippocampus was constant (<10°). Therefore, in all experiments recordings were made from the middle of the pyramidal cell layer (Figures 1A, 1E, and 2A; Figures S1, S2A, S3B, and S4B available online. The electrodes were advanced until sharp wave-ripples (Buzsáki et al., 1992; O'Keefe, 2007), associated with unit firing in the CA1 pyramidal layer, were detected during sleep in the home cage. During subsequent recording sessions, the electrodes were further adjusted to obtain largest amplitude ripples, corresponding to the middle of the pyramidal layer. The phase difference along the transverse axis, i.e., from the subicular end to the fimbrial end of the CA1 pyramidal layer, was approximately 40° (Figure S2).

## Frequency, Power, Coherence, and Phase Shift of Theta Oscillations along the CA1 Septotemporal Axis

For accurate assessment of the changes in LFP theta oscillations along the septotemporal axis of the CA1 region, electrodes were positioned at approximately the same distance from the CA1-subicular border (Figures 2A, S1 [r-25], and S3B). The frequency and regularity of theta oscillations in the dorsal and intermediate hippocampus were similar at all recording sites, with the phase of theta gradually shifting from the dorsal (septal) to intermediate sites of the CA1 layer (Figures 2E, 3F, and S3). Theta waves were phase shifted by approximately a half cycle, i.e., 180° between the septal and ventral (temporal) sites (Figures 3F, 3G, and S4). Theta oscillations were less regular, lower in amplitude, and more intermittent at the ventral sites, with episodes of no recognizable rhythm at times of regular theta oscillation at dorsal locations (Figures 2F, 2G, and S4C; Royer et al., 2010). While coherence of theta waves was relatively high between septal and intermediate sites, it decreased to < 0.5 between septal and ventral sites (Figures 2D and 3E).

Data recorded from 45 histologically verified electrode locations in the dorsal and intermediate hippocampus and 19 histologically verified electrodes from the ventral hippocampus (n = 10 rats) were included in the analysis. For group comparison, the recording sites were categorized into dorsal (0–3.0 mm), intermediate (3.1–6.5 mm), and ventral (8.0–10.0 mm) segments. Because the most ventral electrode in each animal was positioned in a relatively similar plane (between 9$^{th}$ and 10$^{th}$ mm along the septotemporal axis), the ventral CA1 sites were used as reference for coherence and phase shift measurements. The group analysis confirmed that the frequency of theta oscillations remained same along the entire septotemporal axis but differed significantly between REM sleep and maze behavior

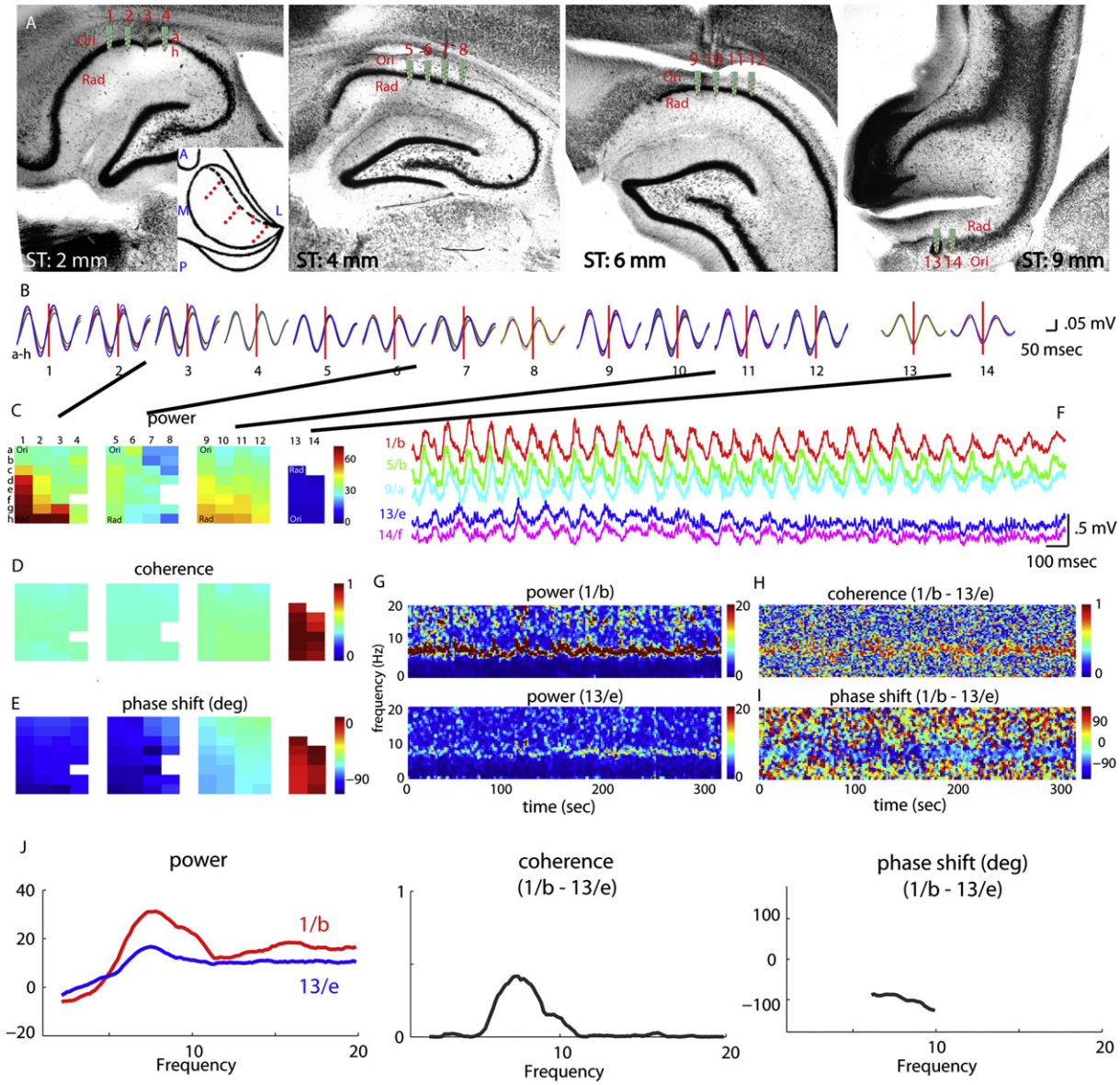


**Figure 2. Three-Dimensional Distribution of Theta Waves in the CA1 Pyramidal Layer**

(A) Inset: top-down view of the right hippocampus. The positions of the recording probes and shanks are shown (red dots). Histological sections were cut along the transverse axis. Silicon probe tips superimposed on the histologically recovered tracks in the dorsal (1st panel), intermediate (2nd and 3rd panels), and ventral (4th panel) segments. Ori, stratum oriens. Rad, stratum radiatum. (a–h) Recording sites on each shank. (B) Average filtered (5–10 Hz) theta waves during REM from all 14 shanks. Average traces from recordings sites (a–h) from the same shank are superimposed. (C–E) Power, coherence, and phase shift as a function of depth (a–h; 20 μm intervals) and transverse axis distance (1-4, 5-8, 9-12, 13-14; shanks are 200 μm apart). Malfunctioning sites are white. (F) Three-second-long wide-band LFP traces during REM theta from selected sites at four septotemporal levels. (G) Time-resolved power spectra during REM periods concatenated over the entire session from the most septal (dorsal) and most temporal (ventral) probes. (H and I) Coherogram (H) and phase shift spectrum (I) calculated between sites shown in (G). (J) Average power, coherence, and phase spectra for sites shown in (G). Phase is shown where coherence is > 0.1.

(RUN) (Figure 3C; REM – DH: 6.97 ± 0.35; IH: 7.07 ± 0.32; VH: 7.00 ± 0.44 Hz, mean and SD, n = 42 sessions in 10 rats; RUN – DH: 7.53 ± 0.31; IH: 7.82 ± 0.26; VH: 7.64 ± 0.32 Hz, mean and SD, n = 28 sessions in 7 rats; recording location effect p = 0.21; state effect: p = 0.008; two-way ANOVA). Identifiable theta oscillations in the ventral hippocampus (see Experimental Procedures) were present at ~60% of the time of prominent theta waves in the dorsal hippocampus (RUN: 63.3% ± 22.11%; REM: 58.1% ± 16.14%; p = 0.31). The power of theta oscillations decreased from dorsal to ventral sites (Figure 3D; REM – DH: 27.24 ± 3.93; IH: 24.43 ± 6.30; VH: 11.87 ± 4.57, mean and SD, n = 42 sessions in 10 rats; RUN – DH: 34.44 ± 2.70; IH: 29.92 ± 2.15; VH: 18.34 ± 3.84, mean and SD, n = 28 sessions in 7 rats; recording location effect, p = 0.003;

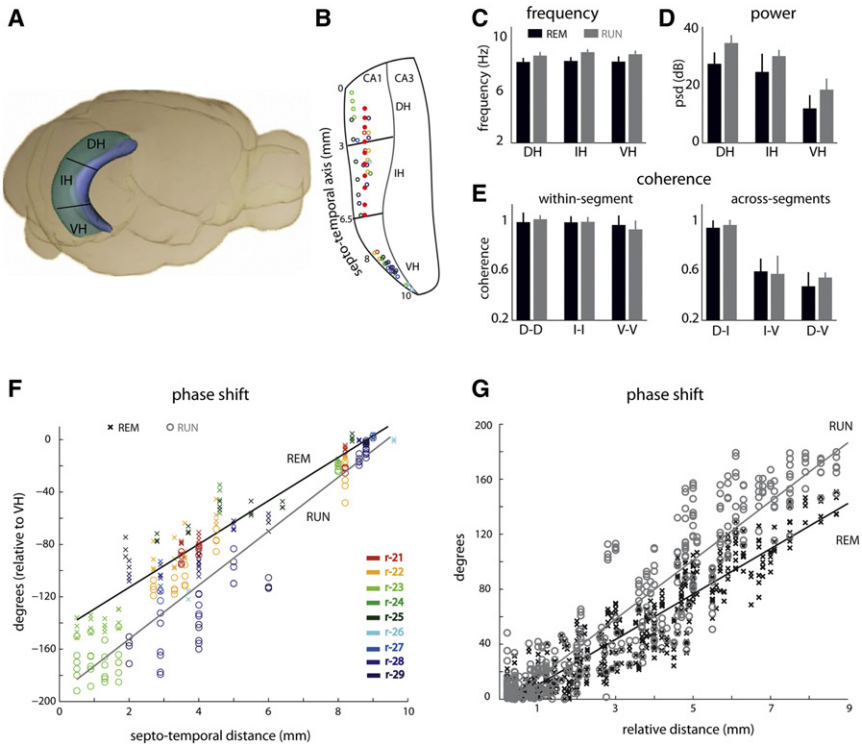


**Figure 3. State and Location-Dependent Features of Phase-Shifting Theta Waves**

(A) Schematics of the dorsal (DH), intermediate (IH), and ventral (VH) divisions of the hippocampus, respectively. (B) Flattened map of the CA1-CA3 regions. Dots indicate the tip of the recording sites in the CA1 pyramidal layer. (C–E) Frequency (C; mean + SD of peak theta frequency, across 42 sessions in ten rats [REM] and 28 sessions in seven rats [RUN]), power (D; mean + SD of average theta power around ± 1 Hz of peak theta frequency), and coherence (E; mean + SD) of theta oscillations in the dorsal (DH; 0–3 mm), intermediate (IH, 3.1–6.5 mm), and ventral (VH, 8.0–10.0 mm) segments of the CA1 region. Results are shown separately from RUN and REM sessions. (F) Phase shift of theta oscillations in individual rats (color coded) as a function of septotemporal distance during REM (x) and RUN (o). In these comparisons, the reference site was the ventral-most electrode. Distances are measured from the septal end of the CA1 pyramidal region (0 mm). Note up to 180° phase shift between the ventral-most and septal-most (dorsal) sites during RUN and significantly less steep phase shift during REM. (G) Theta phase shift as a function of electrode distance. All possible electrode pair comparisons (relative distance) are shown.

two-way ANOVA), and was significantly smaller during REM sleep compared to RUN (state effect, $p = 0.006$, two-way ANOVA). Within-segment coherence in the theta band was high along the long axis and during different behaviors: REM and RUN (Figure 3E, left panel, recording location effect, $p = 0.23$; behavioral state effect, $p = 0.89$; two-way ANOVA). In across-segment comparisons, coherence remained high between dorsal and intermediate sites (Figure 3E, right panel, mean coherence $c > 0.88$ for both REM and RUN), but it was significantly smaller between ventral and intermediate (Figure 3E; $c = 0.46 \pm 0.12$, REM; $c = 0.44 \pm 0.17$, RUN) and ventral and dorsal locations (Figure 3E; $c = 0.32 \pm 0.13$, REM; $c = 0.41 \pm 0.05$, RUN; location effect, $p = 0.009$; two-way ANOVA). Across-segment coherence was similar during RUN and REM ($p = 0.45$; 2-way ANOVA). The slope of theta phase shift versus distance, referenced to the most ventral site in each rat, was significantly more shallow during REM sleep (16.53°/mm; reaching 150° between the most ventral and most septal parts of the hippocampus) than during RUN (20.58°/mm; reaching 180°; $p < 0.00001$; permutation test; Figure 3F). In addition, we calculated phase differences between all possible pairs of recording sites at all septotemporal levels (Figure 3G). The slopes based on these latter comparisons yielded similar values (REM: 16.48°/mm; RUN: 21.36°/mm; $p < 0.00002$; permutation test). The above comparisons were independent of whether epochs were selected based on the presence of theta waves at the ventral (Figures 3F and 3G) or dorsal (Figures S5A and S5B) recording sites. While theta phase shift was monotonous in the septal 2/3rd, it accelerated between the intermediate and ventral segments (Figure S6).

## Theta Phase Locking of Neuronal Firing along the Septotemporal Axis

The temporal shifts of the LFP theta along the septotemporal axis were mirrored by similar phase shifts of unit firing in the CA1 region (Figure 4). At all locations, majority of both multiple units and single pyramidal cells fired preferentially near the trough of the local LFP theta (Figures 4A–4C and 4E). Theta phase preference of ventral neurons was more variable and a fraction of ventral pyramidal cells preferred the peak of the local theta cycle (Figure 4E). This peak preference of ventral neurons was not due to improper positioning of the electrode within the CA1 pyramidal cell layer or misclassification of the unit identity because even well-isolated pyramidal cells, recorded simultaneously by the same probe and referenced to LFP from the same recording site, often showed different theta phase preferences (Figure 4D). Thus, while pyramidal neurons were largely phase locked to the local theta waves, their spiking activity was phase distributed when referenced to the theta cycle recorded from a single site. Assuming an 8 Hz theta signal (125 ms period) and a 10 mm flattened distance between the septal and temporal poles, the half-theta cycle septotemporal phase shift of population unit firing between the two poles corresponds to 0.16 m/s velocity of activity travel, comparable to the speed of traveling activity observed in visual areas (Benucci et al., 2007).

## Comodulation of Theta Power along the Septotemporal Axis and the Effect of Speed on Power

While theta coherence remained moderately high ($c > 0.4$; Figure 3E) along the entire long axis of the CA1 pyramidal layer, theta amplitude (or power) varied extensively (Figures 5A

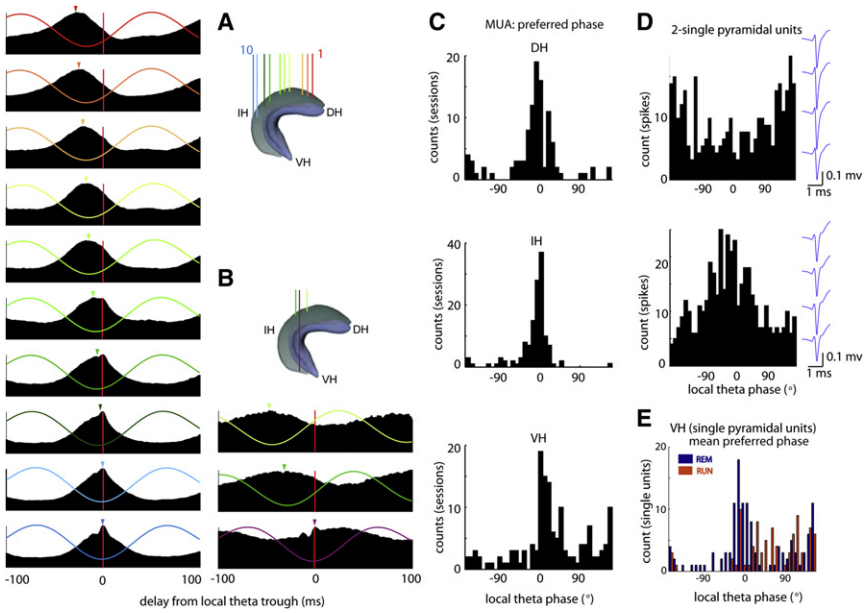


**Figure 4. Theta Phase Shift of Unit Firing along the Septotemporal Axis Is in Register with Phase-Shifting Theta Waves**

(A) Theta trough-triggered LFP (colored line) and corresponding local multiple unit firing histogram (r-11). LFP and units signals are referenced to the theta troughs (zero on the x axis), detected at the most ventral electrode. (B) Similar to (A), field and unit histograms from the dorsal and ventral regions, referenced to the trough of ventral theta (r-28). Note time-shifted LFP average theta waves and corresponding preferred discharge of multiple unit activity at the trough of local theta. (C) Distribution of preferred theta phases of multiple unit firing, referenced to the troughs of local theta waves, in the dorsal (DH), intermediate (IH), and ventral (VH) segments from all animals. Each count is the preferred phase of multiple unit activity (MUA) from an electrode for that session. (D) Two simultaneously recorded putative pyramidal cells from the same tetrode in the ventral CA1 region. Note that of the two neurons, one fires preferentially on the peak and the other at the trough of the local theta cycle, respectively. Waveforms of units (wide band: 1 Hz–5 kHz). (E) Distribution of preferred theta phases of isolated pyramidal neurons from the ventral hippocampus, shown separately for RUN and REM sessions (overlaid). Only cells with significant theta modulation of firing ($p < 0.05$, Raleigh test) were included. Pyramidal cells with < 100 spikes during a session were not included in the analysis.

and 5B). Theta power between sites of the same hippocampal segment (Figure 5C; R > 0.81 REM; R > 0.75 RUN; p = 0.3, two-way ANOVA) and between the dorsal and intermediate segments (Figure 5D; R = 0.66 ± 0.132 REM; R = 0.64 ± 0.134 RUN) covaried reliably. In contrast, covariation of theta power between ventral sites versus intermediate and dorsal hippocampal locations was significantly lower during both REM (Figure 5D; V-I: R = 0.39 ± 0.18; V-D: R = 0.32 ± 0.14; $p < 0.001$; two-way ANOVA) and RUN (Figure 5D; V-I: R = 0.16 ± 0.14; V-D: R = 0.09 ± 0.082; $p < 0.001$; two-way ANOVA). A potential source of theta power modulation in different hippocampal segments is a "speed signal," since the locomotion velocity of the animal is known to affect the amplitude of theta (McFarland et al., 1975). There was a significant correlation between running speed and theta power in the dorsal and intermediate segments (Figures 5E and 5F; Maurer et al., 2005; Montgomery et al., 2009) but not in the ventral segment (Figures 5E and 5F; $p < 0.0001$; ANOVA).

## DISCUSSION

Our results confirm and extend the prediction of Lubenov and Siapas (2009) that the phase of theta waves advances monotonically along the entire long axis of the hippocampus. In their "hippocampal circle" model, the septal and temporal poles are functionally "connected" by a full theta cycle. In contrast, we found ~180° phase offset during exploration and a slower propagation of theta waves during REM, possibly due to the lower frequency of REM theta. A potential source of discrepancy between the two studies is the different axes of phase measurements. In the experiments of Lubenov and Siapas (2009), phase was computed from the combined anteroposterior and mediolateral propagation of theta waves in the dorsal hippocampus and extrapolated to correspond to 240°–360° along the septotemporal axis. Since theta waves travel not only along the long axis but also in the CA1-CA3 direction (Figure S2; Dragoi and Buzsáki, 2006), the simultaneous contribution of the phase shifts in both septotemporal and CA3-subicular axis could have resulted in overestimation of the phase advancement along the LA.

The half-cycle theta shift between the septal and temporal poles should have important functional implications. The orderly temporal offsets between increasing septotemporal levels of the hippocampus result in a sequence of activity maxima of CA1 pyramidal cells, corresponding to the troughs of local theta waves. Combining the delays of activity maxima with spike-timing-dependent plasticity (Markram et al., 1997; Magee and Johnston, 1997), the temporal shifts with distance suggest that the functional connections among neurons at different septotemporal levels are mainly unidirectional during theta oscillations and that neighboring neurons are more strongly connected than distant ones. At the septal and temporal ends of the hippocampus, the half-theta cycle delay (~70 ms) may prevent the association of signals from the poles. These considerations suggest that the intermediate hippocampus is best posed to integrate diverse hippocampal representations (Bast et al., 2009), whereas neurons at the poles broadcast segregated messages to different parts of the neocortex. The relative discontinuity of coherence, phase, and speed correlation between the intermediate and ventral segments also supports this notion. Locomotor velocity had a strong effect on theta power in the dorsal and intermediate hippocampus (McFarland et al., 1975; Montgomery et al., 2009), but this relationship was weak in the temporal segment (Hinman et al., 2011), suggesting that ventral hippocampal neurons are less affected by speed. Because place

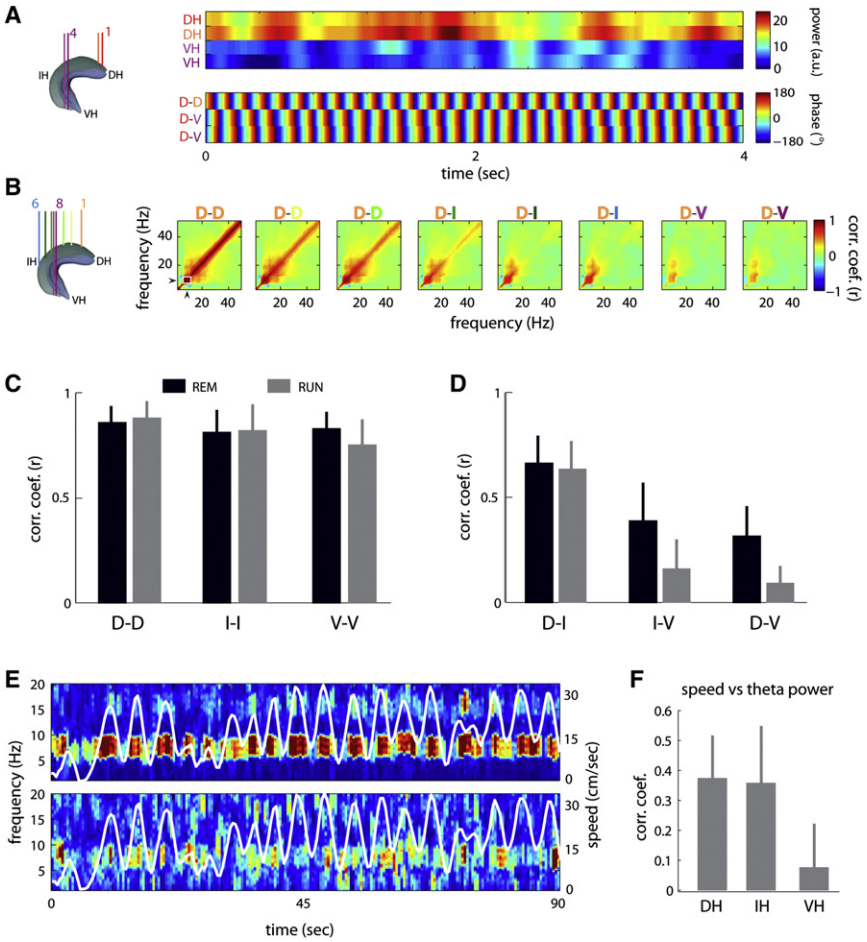


**Figure 5. Power Variability and Speed Dependence of Theta Power**

(A) A 4 s LFP segment showing instantaneous theta amplitude and phase relationships between electrodes in the dorsal and ventral CA1 pyramidal layers (rat-23). Note high theta power correlation between sites in the dorsal CA1 pyramidal layer and virtually independent power fluctuation in sites in the ventral CA1 pyramidal layer (top), while theta phase relationship between dorsal and ventral sites is highly consistent and well preserved during the same period. (B) Power-power correlation between the most dorsal CA1 pyramidal layer recording site (red) and seven other sites in the dorsal (DH), intermediate (IH), and ventral (VH) CA1 pyramidal layers from an example REM session (r-25). (C and D) Group data of power-power correlations. Note high power correlations within the same segments (C) and strongly decreased power correlations between the ventral versus intermediate and dorsal sites (mean + SD). (E) Examples of time-resolved power spectra from the dorsal and ventral CA1 pyramidal layer electrodes (rat-27) and concurrent running speed (superimposed, white) during open field exploration. Note striking correlation of theta power fluctuation with running speed in the dorsal hippocampus and a less reliable relationship in the ventral part. (F) Mean (+ SD) of correlation coefficient values between theta power and speed from all sessions (n = 19 sessions from five rats), grouped as dorsal (DH), intermediate (IH), and ventral (VH) hippocampus. While theta power from the dorsal and intermediate sites was equally and strongly correlated with speed, theta power from the ventral sites showed significantly less correlation with speed than sites in the septal 2/3rd.

cells are speed-controlled oscillators (Geisler et al., 2007; Jeewajee et al., 2008), the diminishing effect of speed supports the hypothesis that inputs to the ventral hippocampus carry largely nonspatial information (Royer et al., 2010).

## Mechanisms of Traveling Theta Waves along the Septotemporal Axis

Traveling LFP waves may arise from multiple distinct mechanisms (Ermentrout and Kleinfeld, 2001). The simplest one requires a single rhythm generator (e.g., the "septal theta pacemaker"; Petsche et al., 1962) and the (fictive) delays would emerge through a progression of increasing time delays, due to the propagation velocity of septo-hippocampal afferents. This mechanism is unlikely to play a significant role for the following reasons. First, it requires precisely tuned delays in multiple collaterals of septal afferents to the various regions of the hippocampus and matching entorhinal cortical inputs. Second, the frequency of theta oscillations depends primarily on the GABAergic neurons of the medial septal area (Lee et al., 1994; Yoder and Pang, 2005), and the conduction velocities of thickly myelinated septo-hippocampal GABAergic neurons (Freund and Antal, 1988) are an order of magnitude faster than the propagation velocity of theta waves (Bilkey and Goddard, 1985). Third, the different septotemporal segments of the hippocampus are not innervated by axons of the same septal neurons. Instead, fibers to the septal two-thirds travel largely in the fimbria and fornix, whereas the temporal segment receives its input through a ventral pathway (Gage et al., 1983). Phase shifts could also arise from a single pacemaker (e.g., medial septum) through delays emerging from a chain of unidirectionally linked groups of neurons (Ermentrout and Kleinfeld, 2001). Another mechanism that could provide delays would be a chain of oscillators residing within the pacemaker itself (e.g., the septal area) and the phase shift observed in the hippocampus would be a reflection of the phase-delayed septal outputs. While this latter solution cannot be fully excluded, it would require a complex temporal coordination of the hippocampal and entorhinal neurons in different regions and layers with appropriate delays.

We hypothesize that traveling theta waves arise from a network of "weakly coupled" (Kopell and Ermentrout, 1986) intrahippocampal and matched entorhinal cortex oscillators. In support of this hypothesis, both the CA3 recurrent system and in vitro slices of the CA3 region can generate theta oscillations (Konopacki et al., 1987; Kocsis et al., 1999). In addition, delays with similar magnitudes documented here have been reported in the isolated CA3 region in vitro (Miles et al., 1988).

The importance of weakly coupled oscillators in traveling waves is illustrated by the spinal cord activity of the lamprey

during swimming (Kopell and Ermentrout, 1986; Cohen et al., 1992). The swim rhythm arises from intersegmental coordination of spinal cord oscillators, connected by local connections with short delays. The dominance of forward swimming is secured by the faster oscillators in the frontal end of the cord (Grillner et al., 1995). By analogy, the oscillation frequencies of place cell assemblies decrease progressively along the septotemporal axis of the hippocampus (Jung et al., 1994; Maurer et al., 2005; Kjelstrup et al., 2008; Royer et al., 2010) and theta oscillating cell groups are coupled by delays (Geisler et al., 2010). Similarly, the oscillation frequencies of medial entorhinal cortex neurons decrease progressively in the dorsoventral direction (Giocomo et al., 2007), providing a frequency match between corresponding entorhinal and hippocampal neurons. Due to the delays, the faster but transient assembly oscillators produce a slower global rhythm, expressed by the coherent LFP oscillation in the entire length of the hippocampus and entorhinal cortex (Geisler et al., 2010). The progressively decreasing excitability of pyramidal neurons along the long axis (Segal et al., 2010) might further contribute to the dominantly septotemporal spread of activity. Finally, septally projecting long-range interneurons (Dragoi et al., 1999; Tóth et al., 1993; Jinno et al., 2007), integrating the spiking activity of pyramidal cells at various septotemporal segments, can serve as conduits to adjust the frequency and level of activity in the medial septum, which, in turn, can coordinate the frequency of global theta oscillations.

## EXPERIMENTAL PROCEDURES

### Animals and Chronic Surgery

Twelve Long-Evans rats (male, 250–400 g, 3–5 months old) were housed individually in transparent Plexiglass cages. Details of surgery and recovery procedures have been described earlier (Csicsvari et al., 1998). After postsurgical recovery, recording wires were lowered over the course of several days in steps of 50 μm until large units and ripple activity were isolated at appropriate depths. The goal was to record, simultaneously, from at least three sites in the dorsal/intermediate CA1 pyramidal layer along the long axis, and from at least 1 site in the CA1 pyramidal layer in the ventral pole (except 2 rats, in which recordings were obtained only along the transverse axis). All experiments were carried out in accordance with protocols approved by the Institutional Animal Care and Use Committee, Rutgers University. For details, see Experimental Procedures.

### Behavioral Training

The animals were handled and trained in two mazes (an open field and a zigzag maze) for at least 2 weeks before surgery (Royer et al., 2010). The animals were water-restricted for 24 hr before the tasks. The same behavioral procedures were used for training and testing. For details, see Experimental Procedures.

### Histological and Physiological Verification of Recording Sites

Since the main goal of the present experiments was to establish theta phase relationships among signals recorded along the LA of the hippocampus, the physical distances between the recording sites rather than the stereotaxic coordinates of the electrodes were measured by taking into account the curvature of the hippocampus. In all figures, the distances of the electrodes are given from the septal end of the hippocampus (e.g., Figure 2). For details, see Experimental Procedures.

### Data Acquisition, Processing, and Analysis

Neurophysiological signals were amplified (1,000×), band pass filtered (1–9 kHz), acquired continuously at 32 kHz on a 128-channel DigiLynx System (24-bit resolution; NeuraLynx, MT) and stored for offline analysis. Raw data were preprocessed using custom-developed suite of programs (Csicsvari et al., 1998).

Spectral analysis was performed on detected theta periods. Theta amplitude and phase differences were measured taking the most ventral channel as reference. All numbers in the format X ± Y stand for mean ± standard deviation, unless otherwise mentioned. For statistics, two-way ANOVA was used unless otherwise mentioned. For details, see Experimental Procedures.

## SUPPLEMENTAL INFORMATION

Supplemental Information includes six figures and Supplemental Experimental Procedures and can be found with this article online at http://dx.doi.org/10.1016/j.neuron.2012.07.015.

## ACKNOWLEDGMENTS

This work was supported by National Institute of Health Grants NS34994 and MH54671, James S. McDonnell Foundation, the Global Institute for Scientific Thinking (G.B.), Marie Curie Fellowship, and the Rosztoczy Foundation (A.B.). We thank J. Csicsvari and S. Montgomery for providing valuable data and M. Bellucio, K. Mizuseki, E. Pastalkova, A. Amir, and D. Sullivan for providing critical comments and insightful suggestions.

Accepted: July 20, 2012
Published: August 8, 2012

## REFERENCES

Amaral, D., and Lavenex, P. (2007). Hippocampal neuroanatomy. In The Hippocampus Book, P. Andersen, R. Morris, D. Amaral, T. Bliss, and J. O'Keefe, eds. (New York: Oxford University Press).

Bannerman, D.M., Grubb, M., Deacon, R.M., Yee, B.K., Feldon, J., and Rawlins, J.N. (2003). Ventral hippocampal lesions affect anxiety but not spatial learning. Behav. Brain Res. *139*, 197–213.

Bast, T., Wilson, I.A., Witter, M.P., and Morris, R.G. (2009). From rapid place learning to behavioral performance: a key role for the intermediate hippocampus. PLoS Biol. *7*, e1000089.

Benucci, A., Frazor, R.A., and Carandini, M. (2007). Standing waves and traveling waves distinguish two circuits in visual cortex. Neuron *55*, 103–117.

Bilkey, D.K., and Goddard, G.V. (1985). Medial septal facilitation of hippocampal granule cell activity is mediated by inhibition of inhibitory interneurones. Brain Res. *361*, 99–106.

Bullock, T.H., Buzsáki, G., and McClune, M.C. (1990). Coherence of compound field potentials reveals discontinuities in the CA1-subiculum of the hippocampus in freely-moving rats. Neuroscience *38*, 609–619.

Buzsáki, G. (2002). Theta oscillations in the hippocampus. Neuron *33*, 325–340.

Buzsáki, G., Horváth, Z., Urioste, R., Hetke, J., and Wise, K. (1992). High-frequency network oscillation in the hippocampus. Science *256*, 1025–1027.

Cenquizca, L.A., and Swanson, L.W. (2007). Spatial organization of direct hippocampal field CA1 axonal projections to the rest of the cerebral cortex. Brain Res. Brain Res. Rev. *56*, 1–26.

Cohen, A.H., Ermentrout, G.B., Kiemel, T., Kopell, N., Sigvardt, K.A., and Williams, T.L. (1992). Modelling of intersegmental coordination in the lamprey central pattern generator for locomotion. Trends Neurosci. *15*, 434–438.

Csicsvari, J., Hirase, H., Czurko, A., and Buzsáki, G. (1998). Reliability and state dependence of pyramidal cell-interneuron synapses in the hippocampus: an ensemble approach in the behaving rat. Neuron *21*, 179–189.

Dolorfo, C.L., and Amaral, D.G. (1998). Entorhinal cortex of the rat: topographic organization of the cells of origin of the perforant path projection to the dentate gyrus. J. Comp. Neurol. *398*, 49–82.

Dong, H.W., Swanson, L.W., Chen, L., Fanselow, M.S., and Toga, A.W. (2009). Genomic-anatomic evidence for distinct functional domains in hippocampal field CA1. Proc. Natl. Acad. Sci. USA *106*, 11794–11799.

Dragoi, G., and Buzsáki, G. (2006). Temporal encoding of place sequences by hippocampal cell assemblies. Neuron *50*, 145–157.

Dragoi, G., Carpi, D., Recce, M., Csicsvari, J., and Buzsáki, G. (1999). Interactions between hippocampus and medial septum during sharp waves and theta oscillation in the behaving rat. J. Neurosci. *19*, 6191–6199.

Ermentrout, G.B., and Kleinfeld, D. (2001). Traveling electrical waves in cortex: insights from phase dynamics and speculation on a computational role. Neuron *29*, 33–44.

Freund, T.F., and Antal, M. (1988). GABA-containing neurons in the septum control inhibitory interneurons in the hippocampus. Nature *336*, 170–173.

Gage, F.H., Björklund, A., and Stenevi, U. (1983). Reinnervation of the partially deafferented hippocampus by compensatory collateral sprouting from spared cholinergic and noradrenergic afferents. Brain Res. *268*, 27–37.

Geisler, C., Robbe, D., Zugaro, M., Sirota, A., and Buzsáki, G. (2007). Hippocampal place cell assemblies are speed-controlled oscillators. Proc. Natl. Acad. Sci. USA *104*, 8149–8154.

Geisler, C., Diba, K., Pastalkova, E., Mizuseki, K., Royer, S., and Buzsáki, G. (2010). Temporal delays among place cells determine the frequency of population theta oscillations in the hippocampus. Proc. Natl. Acad. Sci. USA *107*, 7957–7962.

Giocomo, L.M., Zilli, E.A., Fransén, E., and Hasselmo, M.E. (2007). Temporal frequency of subthreshold oscillations scales with entorhinal grid cell field spacing. Science *315*, 1719–1722.

Grillner, S., Deliagina, T., Ekeberg, O., el Manira, A., Hill, R.H., Lansner, A., Orlovsky, G.N., and Wallén, P. (1995). Neural networks that co-ordinate locomotion and body orientation in lamprey. Trends Neurosci. *18*, 270–279.

Hampson, R.E., Simeral, J.D., and Deadwyler, S.A. (1999). Distribution of spatial and nonspatial information in dorsal hippocampus. Nature *402*, 610–614.

Hinman, J.R., Penley, S.C., Long, L.L., Escabí, M.A., and Chrobak, J.J. (2011). Septotemporal variation in dynamics of theta: speed and habituation. J. Neurophysiol. *105*, 2675–2686.

Ishizuka, N., Weber, J., and Amaral, D.G. (1990). Organization of intrahippocampal projections originating from CA3 pyramidal cells in the rat. J. Comp. Neurol. *295*, 580–623.

Jeewajee, A., Barry, C., O'Keefe, J., and Burgess, N. (2008). Grid cells and theta as oscillatory interference: electrophysiological data from freely moving rats. Hippocampus *18*, 1175–1185.

Jinno, S., Klausberger, T., Marton, L.F., Dalezios, Y., Roberts, J.D., Fuentealba, P., Bushong, E.A., Henze, D., Buzsáki, G., and Somogyi, P. (2007). Neuronal diversity in GABAergic long-range projections from the hippocampus. J. Neurosci. *27*, 8790–8804.

Jung, M.W., Wiener, S.I., and McNaughton, B.L. (1994). Comparison of spatial firing characteristics of units in dorsal and ventral hippocampus of the rat. J. Neurosci. *14*, 7347–7356.

Kjelstrup, K.G., Tuvnes, F.A., Steffenach, H.A., Murison, R., Moser, E.I., and Moser, M.B. (2002). Reduced fear expression after lesions of the ventral hippocampus. Proc. Natl. Acad. Sci. USA *99*, 10825–10830.

Kjelstrup, K.B., Solstad, T., Brun, V.H., Hafting, T., Leutgeb, S., Witter, M.P., Moser, E.I., and Moser, M.B. (2008). Finite scale of spatial representation in the hippocampus. Science *321*, 140–143.

Kocsis, B., Bragin, A., and Buzsáki, G. (1999). Interdependence of multiple theta generators in the hippocampus: a partial coherence analysis. J. Neurosci. *19*, 6200–6212.

Konopacki, J., Bland, B.H., and Roth, S.H. (1987). Phase shifting of CA1 and dentate EEG theta rhythms in hippocampal formation slices. Brain Res. *417*, 399–402.

Kopell, N., and Ermentrout, G.B. (1986). Symmetry and phase locking in chains of weakly coupled oscillators. Commun. Pure Appl. Math. *39*, 623–660.

Lee, M.G., Chrobak, J.J., Sik, A., Wiley, R.G., and Buzsáki, G. (1994). Hippocampal theta activity following selective lesion of the septal cholinergic system. Neuroscience *62*, 1033–1047.

Li, X.G., Somogyi, P., Ylinen, A., and Buzsáki, G. (1994). The hippocampal CA3 network: an in vivo intracellular labeling study. J. Comp. Neurol. *339*, 181–208.

Lubenov, E.V., and Siapas, A.G. (2009). Hippocampal theta oscillations are travelling waves. Nature *459*, 534–539.

Magee, J.C., and Johnston, D.A. (1997). A synaptically controlled, associative signal for Hebbian plasticity in hippocampal neurons. Science *275*, 209–213.

Markram, H., Lübke, J., Frotscher, M., and Sakmann, B. (1997). Regulation of synaptic efficacy by coincidence of postsynaptic APs and EPSPs. Science *275*, 213–215.

Maurer, A.P., Vanrhoads, S.R., Sutherland, G.R., Lipa, P., and McNaughton, B.L. (2005). Self-motion and the origin of differential spatial scaling along the septo-temporal axis of the hippocampus. Hippocampus *15*, 841–852.

McFarland, W.L., Teitelbaum, H., and Hedges, E.K. (1975). Relationship between hippocampal theta activity and running speed in the rat. J. Comp. Physiol. Psychol. *88*, 324–328.

Miles, R., Traub, R.D., and Wong, R.K. (1988). Spread of synchronous firing in longitudinal slices from the CA3 region of the hippocampus. J. Neurophysiol. *60*, 1481–1496.

Montgomery, S.M., Betancur, M.I., and Buzsáki, G. (2009). Behavior-dependent coordination of multiple theta dipoles in the hippocampus. J. Neurosci. *29*, 1381–1394.

Moser, E.I., Kropff, E., and Moser, M.B. (2008). Place cells, grid cells, and the brain's spatial representation system. Annu. Rev. Neurosci. *31*, 69–89.

O'Keefe, J. (2007). Hippocampal Neurophysiology in the behaving animal. In The Hippocampus Book, P. Andersen, R. Morris, D. Amaral, T. Bliss, and J. O'Keefe, eds. (New York: Oxford University Press).

O'Keefe, J., and Nadel, L. (1978). The Hippocampus as a Cognitive Map (USA: Oxford University Press).

Petrovich, G.D., Canteras, N.S., and Swanson, L.W. (2001). Combinatorial amygdalar inputs to hippocampal domains and hypothalamic behavior systems. Brain Res. Brain Res. Rev. *38*, 247–289.

Petsche, H., Stumpf, C., and Gogolak, G. (1962). [The significance of the rabbit's septum as a relay station between the midbrain and the hippocampus. I. The control of hippocampus arousal activity by the septum cells]. Electroencephalogr. Clin. Neurophysiol. *14*, 202–211.

Risold, P.Y., and Swanson, L.W. (1996). Structural evidence for functional domains in the rat hippocampus. Science *272*, 1484–1486.

Royer, S., Sirota, A., Patel, J., and Buzsáki, G. (2010). Distinct representations and theta dynamics in dorsal and ventral hippocampus. J. Neurosci. *30*, 1777–1787.

Segal, M., Richter-Levin, G., and Maggio, N. (2010). Stress-induced dynamic routing of hippocampal connectivity: a hypothesis. Hippocampus *20*, 1332–1338.

Small, S.A. (2002). The longitudinal axis of the hippocampal formation: its anatomy, circuitry, and role in cognitive function. Rev. Neurosci. *13*, 183–194.

Thompson, C.L., Pathak, S.D., Jeromin, A., Ng, L.L., MacPherson, C.R., Mortrud, M.T., Cusick, A., Riley, Z.L., Sunkin, S.M., Bernard, A., et al. (2008). Genomic anatomy of the hippocampus. Neuron *60*, 1010–1021.

Tóth, K., Borhegyi, Z., and Freund, T.F. (1993). Postsynaptic targets of GABAergic hippocampal neurons in the medial septum-diagonal band of broca complex. J. Neurosci. *13*, 3712–3724.

Wiener, S.I. (1996). Spatial, behavioral and sensory correlates of hippocampal CA1 complex spike cell activity: implications for information processing functions. Prog. Neurobiol. *49*, 335–361.

Witter, M.P., Groenewegen, H.J., Lopes da Silva, F.H., and Lohman, A.H. (1989). Functional organization of the extrinsic and intrinsic circuitry of the parahippocampal region. Prog. Neurobiol. *33*, 161–253.

Yoder, R.M., and Pang, K.C. (2005). Involvement of GABAergic and cholinergic medial septal neurons in hippocampal theta rhythm. Hippocampus *15*, 381–392.